Journal of Computational Applied Mechanics 2025, 56(1): 127-144

DOI: 10.22059/jcamech.2024.376821.1102

RESEARCH PAPER

# Geometric configuration and parametric evaluation of auxetic meta-materials for enhanced plastic energy dissipation in blast scenarios

Bhanu Murthy M [a], Ramu M [a, *], Chidambara Raja S [b], Pierre-thomas Doutre [c], Frederic Vignat [c]

[a] *Department of Mechanical Engineering, Amrita School of Engineering, Coimbatore, Amrita Vishwa Vidyapeetham, India*

[b] *Indian Oil Corporation Limited, Coimbatore*

[c] *School of Industrial Engineering, Grenoble Institute of Technology, Grenoble, France*

**Abstract**

**The prevailing risk factors and explosion scenarios in Electric Vehicles (EVs) necessitated this research to focus on the analysis and optimization of auxetic patterns encompassing re-entrant, double re-entrant, and triangular structures under blast loading conditions. In this study, a comprehensive blast analysis has been conducted numerically using ABAQUS on auxetic meta-materials featuring re-entrant, double re-entrant, and triangular structures with varying strut angles (85°, 80°, 75°) and strut thickness. Their performances have been compared among them and also with a traditional solid plate. Among these auxetic structures, the double re-entrant structure with 85º strut angle and 0.2 mm strut thickness outperformed other auxetic structures with a minimal bottom plate displacement of 3.4 mm and plastic dissipation energy of 0.171 kJ. The consistent behavior of these structures has been substantiated by conducting blast analysis with a reduced stand-off distance of 30 mm. The simulation results are then compared with the results of the 50 mm stand-off distance for deformation, plastic dissipation energy, and velocity.**

**Keywords:** Auxetic metamaterials; Air blast; Auxetic structures; EV batteries; Blast resistance.

## 1. Introduction

Mechanical metamaterials are artificial structures with extraordinary properties, often inspired by nature and biomaterials. They exhibit remarkable mechanical properties, such as zero or negative Poisson's ratios, negative stiffness, and nonlinear behavior, primarily determined by their geometry rather than chemical composition. These materials can be designed to have negative Poisson ratios making them efficient energy absorbers and less susceptible to fatigue. Auxetic materials, which contract under compression and expand under tension, are valuable in various fields including smart filters, sensors, medical devices, and protective equipment.

Various types of cellular metamaterials have been discovered to predict auxetic behavior and optimize geometric properties, but their utility is often limited to specific dimensions [1-8]. Mengqi Wan et al. [9] explored novel 4D-printed programmable metamaterials, including triangular, square, and honeycomb lattice structures.

* Corresponding author. Tel.: +91 98658 97767, *E-mail address:* m_ramu@cb.amrita.edu

These materials exhibit adjustable mechanical properties, such as auxetic behavior and shape memory effects, enabling potential applications in fields such as flexible electronics, biomedicine, and biomedical scaffolds. Xiaozhou Xin et al. [10] developed 4D-printed chiral metamaterials with tunable, programmable, and reconfigurable properties, overcoming limitations of traditional auxetic metamaterials, and enabling biomimetic stress-deformation behaviors akin to tissues or organs, thereby offering promising applications in tissue engineering and programmable flexible electronics. Xiang Li et al. [11] introduced novel 2D metamaterial structures exhibiting negative Poisson's ratio (NPR) and negative thermal expansion (NTE) properties, showcasing the potential for engineering applications such as smart sensors and electronic components. These properties were achieved through micro-scale mechanical experiments and numerical simulations. Lingling Wu et al. [12] proposed a novel method for achieving two- and three-dimensional negative thermal expansion metamaterials via antichiral structures, this study contributes to the advancement of materials science by offering a practical approach to obtaining materials with tunable negative thermal expansion properties. Xin Ren et al. [13] proposed a 3D design for buckling-induced auxetic metamaterials, utilizing a unit cell composed of a solid sphere and three cuboids, revealing challenges in achieving reliable 3D auxetic behavior. Ai et al. [14] studied four types of three-dimensional (3-D) metallic metamaterials characterized by adjustable thermo-mechanical properties. These materials demonstrate cubic symmetry, necessitating three independent elastic constants and one coefficient of thermal expansion. Sicong Shan et al. [15] created isotropic 2D auxetic materials crucial for versatile applications. This can be achieved by perforating sheets with elongated cuts in specific symmetrical patterns, resulting in tunable behavior even under substantial deformation. Faris et al. [16] conducted a study on sandwich structures as energy absorbers for high dynamic loading situations, it was emphasized that such structures, including those with foam and architected cores, exhibit promising crashworthiness and blast-related performance due to their ability to absorb high kinetic energy through irreversible deformation. Yi Luo et al. [17] examined the impact resistance of sandwich panels with varying Poisson's ratios, determined by diverse topologies including re-entrant, semi-re-entrant, and convex cells. Gabriele et al. [18] investigated sandwich panels with auxetic lattice cores and metallic facets through numerical simulations and parametric analyses. Jakub Michalski et al. [19] compared auxetic materials' resistance to dynamic loads, attributing their enhanced performance to their negative Poisson's ratio (PR). Impact tests demonstrated the potential for auxetic structures to replace traditional hexagonal honeycomb cores in puncture protection. Shuai Yue et al. [20] proposed a projectile-in-motion setup utilizing non-metallic material and multiple damage elements to examine the impact dynamics on the internal structure of an artificial satellite, represented by a honeycomb sandwich panel and multi-layer plates. Gabriele et al. [21] conducted numerical studies on sandwich panels with auxetic cores and metal facets, demonstrating superior blast resistance by absorbing double the impulsive energy and reducing back facet velocity by up to 70% compared to monolithic panels.

Sayed M et al. [22] examined the behavior of prospective materials that can withstand the abrupt stresses put on them by explosive substances, using honeycomb sandwich panels which are widely utilized for blast-resistant structural components. Zheng Kai et al. [23] proposed an innovative approach employing Lagrange particles and Euler meshes to model the dynamic response and failure progression of steel structures subjected to explosive loading. Faizal et al. [24] performed experimental and computational approaches for assessing the performance of auxetic core infills in sandwich panels against underground charges, especially 160 grams of PE4 explosive. Hong Lin et al. [25] developed a numerical enhancement strategy for the topological arrangements and geometric characteristics of unit cells in honeycomb structures and created an improved design for an offshore blast wall with different honeycomb cores. Shujian Yao et al. [26] used a dimensional analysis and numerical simulations to provide a quick approach for estimating the range of damage incurred by metal box structures exposed to internal blast forces. Comprehensive computational research was done by Nejc Novak et al. [27] on the behaviour of sandwich composite panels with auxetic cores under blast loading. H.N.G. Wadley et al. [28] investigate the use of cellular materials for both passive and active blast overpressure reduction. Montazeri et. al. [29] designed three heterogenous re-entrant honeycombs, inspired by natural and material structures, exhibit enhanced mechanical properties surpassing benchmarks, particularly in specific energy absorption and stiffness, making them promising for construction and automotive industries. Hajighasemi et. al. [30] developed a novel geometric-based method to design structures with nonlinear elastic response, utilizing smart materials and external stimuli to alter specific properties such as the effective Young's modulus, demonstrated through numerical simulations and experimental validation via FDM 3D printing, resulting in a potential increase of up to 142% in the effective Young's modulus. Amin et al. [31] concluded that load bearing capacity, Specific energy absorption, flexibility, and flexural modulus of the honeycomb structure could be enhanced by tailoring them with a hybrid geometry lattice. Their architected hybrid geometry honeycombs with various Poisson's ratios is suitable for automotive applications and construction industries. A numerical model was developed to predict the performance of piezoelectric energy harvester in beam configuration with respect to experimental test and the effect of implementing auxetic substrate. Isotropic and auxetic substrates are used for making beams. More charges are generated in both in-plane directions by exciting

piezo using auxetic substrate [32].

Numerous researchers have explored the mechanical and structural characteristics of auxetic metamaterials, including their negative Poisson's ratio, negative thermal expansion, and deformation properties. However, there is a notable gap in research specifically targeting the development and enhancement of auxetic metamaterials for dynamic loading scenarios. Addressing this gap, our study investigates three distinct structures: re-entrant, double re-entrant, and triangular. Notably, the double re-entrant structure emerges as a unique design chosen for its potential to explore dynamic characteristics across various strut angles, strut thicknesses, and standoff distances under blast scenarios concerning deformation, velocity, and plastic dissipation energy, compared with that of a solid plate. Subsequently, optimization concerning strut angle and strut thickness has been done for all three structures. The double re-entrant structure demonstrated remarkable potential and uniqueness in withstanding blast loads. This signifies its promising suitability for applications such as electric vehicle battery shielding [33-35]. Methodology and Comprehensive numerical models are discussed in the following sections followed by findings and discussions.

## 2. Methodology

### *2.1. Modeling auxetic unit cell*

In this study, structures such as re-entrant, double re-entrant, and triangular are picked to display the effect of Negative Poisson's Ratio (NPR). The re-entrant unit cell geometric configurations are defined by angle, θ (85$^o$, 80$^o$, 75$^o$), L1 is the horizontal length, L2 is the vertical length, and H is the total length of the unit cell (Fig.1). The fundamental re-entrant structure is shown in Fig 1(a) for angle θ as 85$^o$, L1 as 5 mm, L2 as 5 mm, and the strut thickness 't' as 0.2 mm. The double re-entrant unit cell configurations are defined by angle, θ1 (85$^o$, 80$^o$, 75$^o$), θ2 (85$^o$, 80$^o$, 75$^o$), L1 is the horizontal length, L2 is the vertical length and H is the total length of the unit cell. The fundamental double re-entrant structure is depicted in Fig 1(b) with angles θ1 as 85$^o$, θ2 as 85$^o$, L1 as 15 mm, L2 as 15 mm, C1 as 5 mm, C2 as 5 mm, C3 as 5 mm, and strut thickness t as 0.2 mm. The triangular unit cell configurations are defined by angles, θ1 (65$^o$), θ2 (85$^o$, 80$^o$, 75$^o$), L1 is the horizontal length, L2 is the vertical length. The fundamental triangular structure is presented in Fig 1(c) with angles θ1 = 65$^o$, θ2 = 5$^o$ L1 = 5 mm, L2 = 5 mm, C1 = 2.3 mm, C2 = 0.2 mm, C3 = 0.3 mm and the strut thickness defined as t = 0.2 mm.

In the initial stage of the research, a careful investigation of three auxetic patterns (re-entrant, double re-entrant, and triangle structures) and their innate auxetic properties, known as negative PR behavior has been done. Three distinct strut angles 85°, 80°, and 75° are chosen for these structures and modelled. To enable precise simulations, the mesh size of these models is optimized through a mesh independence study. Subsequently, numerical simulations are carried out under blast scenarios for the selected auxetic structures.

Several key parameters, such as bottom plate deformation, velocity, and plastic dissipation energy are examined to assess the effectiveness of these structures in withstanding blast forces and compared with traditional solid plates. Based on the simulation results, the optimized strut angle of individual structures has been concluded. Among these three distinct structures with optimized strut angles, computational simulations are performed to reveal the best-performing structure concerning optimum values of deformation, plastic dissipation energy, and velocity parameters.

The parametric analyses and optimization of the auxetic structures have been carried out by varying the strut thickness from 0.2 mm to 0.5 mm of individual structures and their effects concerning overall deformation, plastic dissipation energy, and velocity are studied. Finally, the structural consistency has been studied by reducing the stand-off distance to 30 mm, and their dynamic effects are analyzed. The simulation results are then compared with the results of the 50 mm stand-off distance for deformation, plastic dissipation energy, and velocity.

To validate the numerical results of this study, the blast loading model outlined in [21] is replicated. The monolithic plate which is used by the above reference has specific dimensions: a thickness of 4.6 mm and 300×300 mm. The initial impact of the shock wave occurred at the center of the plate, located at the corner of the quarter plate. Through the present modeling and analysis, a maximum displacement of 24.3mm along the negative y-axis and a velocity of 90.1m/s was obtained which is almost identical with the results of the reference (maximum displacement as 24mm, and velocity as 89m/s [21]. This meticulous validation process underscores the reliability of the present numerical approach.

### *2.2. Evaluation of Poisson's ratio for auxetic structures*

The Effective Poisson's Ratio (EPR) $\nu_{zx}$ of the auxetic unit cell is characterized by the ratio of transverse engineering strain on account of horizontal deformation to the axial engineering strain derived from the corresponding vertical deformation [21]. Eq (1) provides the general expression to calculate PR for the auxetic structures (re-entrant, double re-entrant, and triangular).

$$\upsilon_{zx} = -\frac{\varepsilon_x}{\varepsilon_z} \tag{1}$$

$\varepsilon_x$ is the transverse strain, $\varepsilon_z$ is the longitudinal strain, and $\nu_{zx}$ is the PR. In line with the procedures given in the reference [21], the auxetic structures are constructed using ABAQUS software, with the top surface of the unit cell undergoing a uniform static loading and the bottom surface of the unit cell being constrained. From the simulation, deformations, and PR are obtained numerically. The PR values of the auxetic structures with tailored angles are given in Table 1.

Among various auxetic structures, the unit cell for re-entrant, and double re-entrant structure with 85° angle yields the highest EPR value, while the triangular structure exhibits its highest EPR value at an angle of 75°.

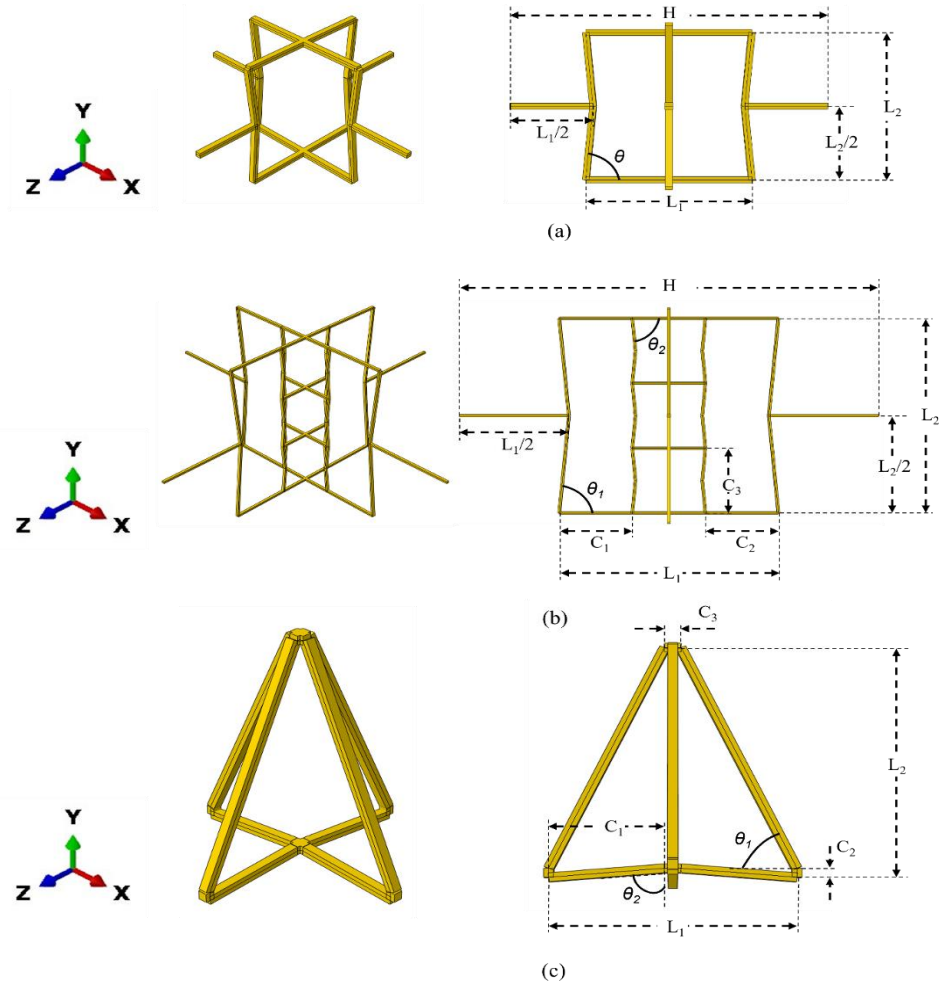


**Fig 1: Three-dimensional auxetic unit cell's fundamental design, a) Re-entrant structure, b) Double re-entrant structure, c) Triangular structure.**

**Table 1: EPR values of auxetic structures.**

| Angle (θ) | Re-entrant (PR $\nu_{zx}$) | Double re-entrant (PR $\nu_{zx}$) | Triangular (PR $\nu_{zx}$) |
|---|---|---|---|
| 85° | -3.2 | -5.5 | -0.26 |
| 80° | -2.4 | -3.1 | -0.53 |
| 75° | -1.9 | -2.1 | -0.78 |

*2.3. Finite element modeling and mesh convergence analysis for auxetic structures*

A mesh convergence analyses have been performed for auxetic structures with four-node shell elements (S4R)

using ABAQUS software to evaluate the accuracy and reliability of the simulations. For re-entrant structure, the meshing is carried out from coarser to finer and then plastic dissipation energy is calculated. The results of the calculated plastic dissipation energy values for different mesh sizes are graphically represented in Fig 2.

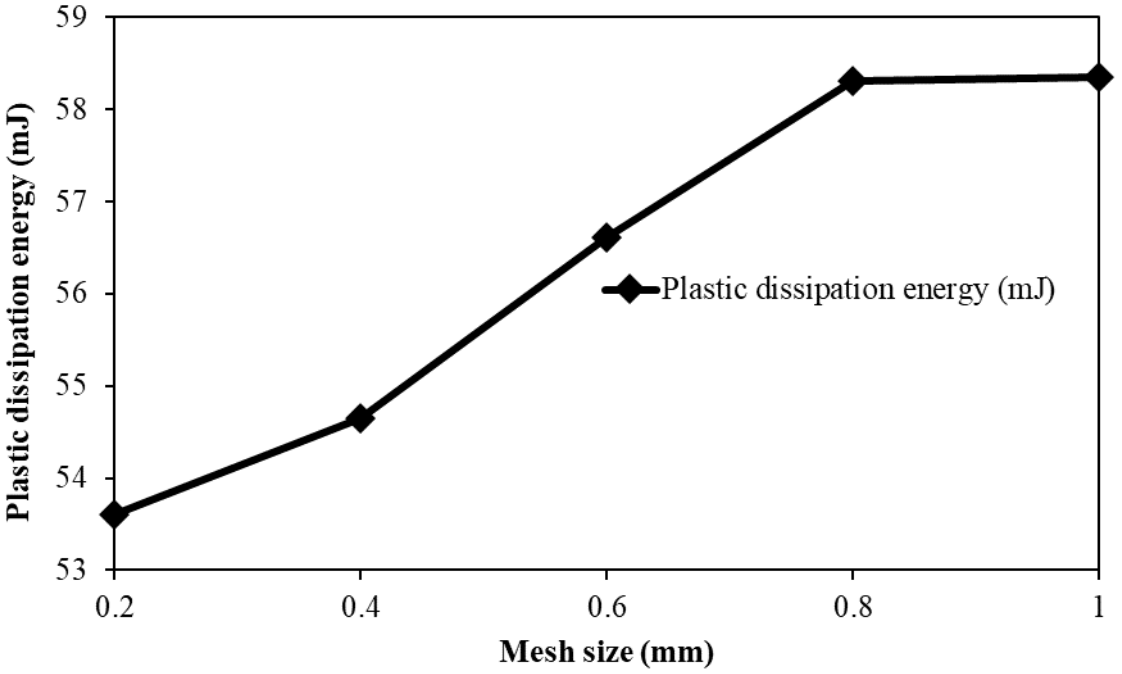


**Fig 2: Plastic dissipation energy (mJ) versus mesh size (mm)**

The graph shown in Fig 2 demonstrates that 0.8 mm mesh size produces stable and consistent simulation results. Conversely, using coarser meshes above 0.8 mm caused a discernible deviation in the results, while finer meshes (0.2 mm, 0.4 mm, and 0.6 mm) considerably raised computational requirements without delivering a substantial enhancement in accuracy. To sustain the accuracy of predicted results and reasonable computational time, 0.8 mm mesh is employed for the entire structures.

### *2.4. Modeling of auxetic sandwich plate*

The re-entrant structure with an angle of 85º is organized into three layers to be considered as a sandwich plate subjected to a blast scenario. The core comprises a total of 2187 individual unit cells calculated as 27 mm ×27 mm × 3 mm with a volume of 255×255×15 $mm^3$ positioned between two plates. The schematic design of the model is shown in Fig 3.

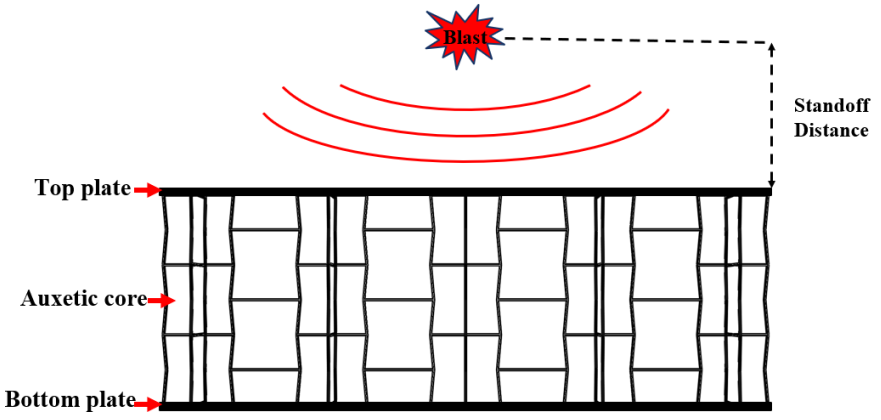


**Fig 3: Schematic design for auxetic sandwich plate.**

Annealed SS304 [21, 36, 37] has been employed for the entire auxetic sandwich plate, and Table 2 provides the

Johnson Cook parameters of annealed stainless steel 304.

**Table 2: Johnson Cook parameters of Annealed SS304 [21]**

| Parameter | Value |
|---|---|
| Youngs modulus, $E$ (GPa) | 200 |
| Poisson's ratio, $\nu$ | 0.3 |
| Yield stress, $A$ (MPa) | 310 |
| Strain hardening, $B$ (MPa) | 1000 |
| Strain hardening exponent, $n$ | 0.65 |
| Strain rate constant, $C$ | 0.07 |
| Thermal softening constant, $m$ | 1 |
| Reference strain rate, $\dot{\varepsilon}_o$ ($s^{-1}$) | 1 |
| Density $\rho$ ($kg/m^3$) | 7900 |
| Melting temperature, $T_m$ (K) | 1673 |
| Room temperature, $T_r$ (K) | 293 |

The unit cells are modeled with shell elements before being assembled; each unit cells are then structured into three layers and merged into a single instance. Specifically, the re-entrant core was modeled with 116154 four-node shell elements (S4R) employed with a global mesh size of 0.8 mm, and the diagonal struts were made with 6 shell elements. The top and bottom plates are modeled with 10404 four-node shell elements (S4R) with a 2.5 mm global mesh size [21]. An equivalent solid plate of the same mass is also modeled to compare its behavior with the auxetic structures and is summarized in Table 3. The thickness of the solid plate is set to 1.1 mm. This solid plate was modeled with a mesh size of 6 mm [21], consisting of 1849 four-node shell elements (S4R).

**Boundary conditions applied for the analysis:** All four edges of the top and bottom plates are fixed.

**Table 3 Structural metrics for various designs**

| Structure | Angle (θ) | Equivalent mass (kg) |
|---|---|---|
| Re-entrant | 85°,80°,75° | 0.54~0.55 |
| Double re-entrant | 85°,80°,75° | 0.525 |
| Triangular | 85°,80°,75° | 0.54~0.55 |
| Solid | - | 0.565 |

*2.5. Air blast*

The Conventional Weapons Effects (CONWEP) is employed to calculate blast loads. By inputting the type and quantity of explosives, CONWEP can estimate the pressure exerted by the resulting blast wave over time. This model forecasts air blast features caused by explosive detonations, with pressure decreasing over time in an exponential structure as given in Eq (2) [38].

$$P(t) = P_{\max}\left(1-\left[\frac{(t-T_a)}{T_o}\right]\right)e^{\left(-A\left[\frac{(t-T_a)}{T_o}\right]\right)} \quad (2)$$

In equation (2), P(t) symbolizes the pressure (MPa) at time 't'; $P_{max}$ denotes maximum pressure (MPa); $T_a$ represents arrival time (ms); $T_o$ indicates positive phase duration (ms); A the exponential decay. According to the details furnished in the reference [39], 61.72kJ of thermal energy which is equivalent to 5.57g of TNT

(Trinitrotoluene), can be liberated by a fully charged fresh 18650 lithium-ion battery. Therefore, the study incorporates a 5.57g spherical TNT explosive charge positioned at a 50 mm standoff distance from the top plate. This encompasses a reflected stress wave's maximum pressure, registering at 92.7MPa, along with a total reflected impulse of 3.5MPa-ms. The stress wave arrival time onto the structure is recorded at 0.01ms, and the positive phase exhibits a duration of 0.032 ms.

The above blast loading parameters are then integrated into the incident wave property in the interaction module. The evaluation of the performance of auxetic structures involves assessing the dissipated plastic energy, maximum deformation, and the evolution of central velocity in the bottom plate. Tie contact is employed to knit the auxetic sandwich plate to reduce the mesh complexity. Fixed boundary conditions are applied on the edges of both top and bottom plates.

## 3. Numerical Analysis and Discussions

### *3.1. Assessment of the blast-resistant capabilities of the auxetic structures*

Simulations are carried out for the designed auxetic structures (re-entrant structure, double re-entrant, and triangular structure (with 85º, 80º, 75º strut angles). The blast load was 5.57 g of TNT with an equivalent impulse load of 3.5 MPa-ms. Fig 4 displays the cross-sectional view of deformations for re-entrant, double re-entrant, triangular auxetic structures with 85º strut angle as well as solid plate. The S, mises stress shown in the Fig 4 is expressed in MPa. Through the analysis, it is found that the top plate undergone plastic deformation by compressing the core, and the bottom plate remains unaffected. At the outset, considerable stress accumulates predominantly at the centre of the plate because of the impact blast wave. However, over a time, these stresses progressively disseminate and disperse throughout the entire plate, aligning with the trajectory of the transmitted shockwave. This phenomenon embodies the dynamic response of the plate to the abrupt and potent external forces imposed by the blast wave, ultimately yielding a stress distribution across the structure.

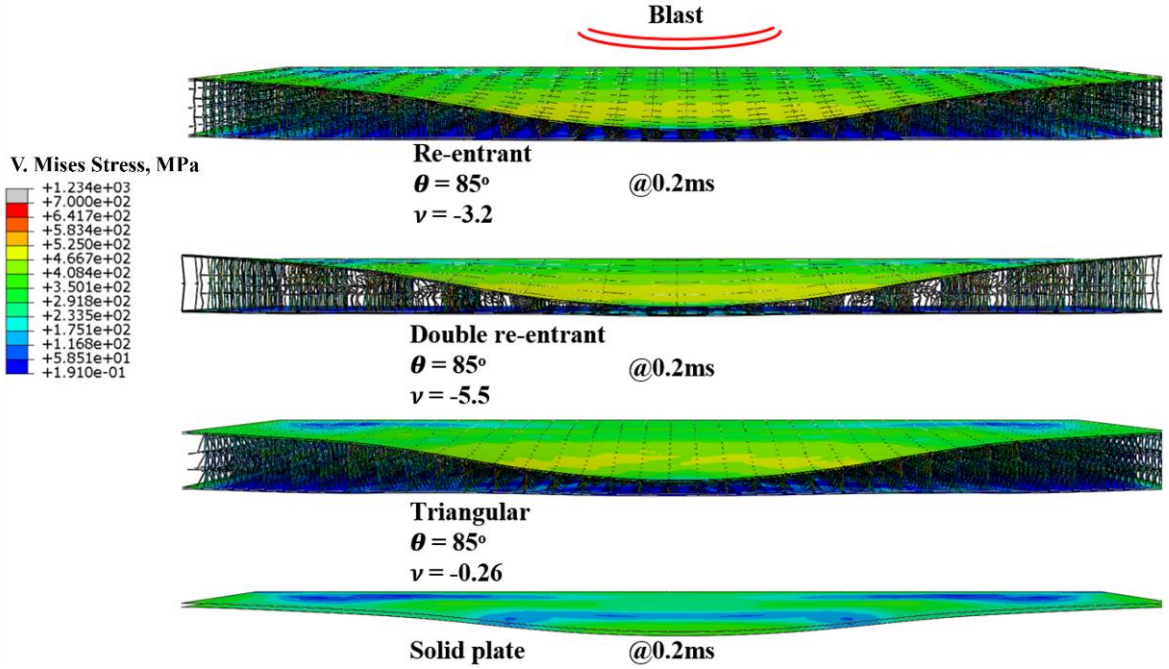


**Fig 4: Deformations of re-entrant, double re-entrant, triangular structures and solid plate (S, Mises stress in MPa)**

#### *3.1.1. Cumulative assessment of re-entrant structures*

Figure 5(a) illustrates the deformations of bottom plates for re-entrant structures with strut angles 85º, 80º, 75º, and solid plate.

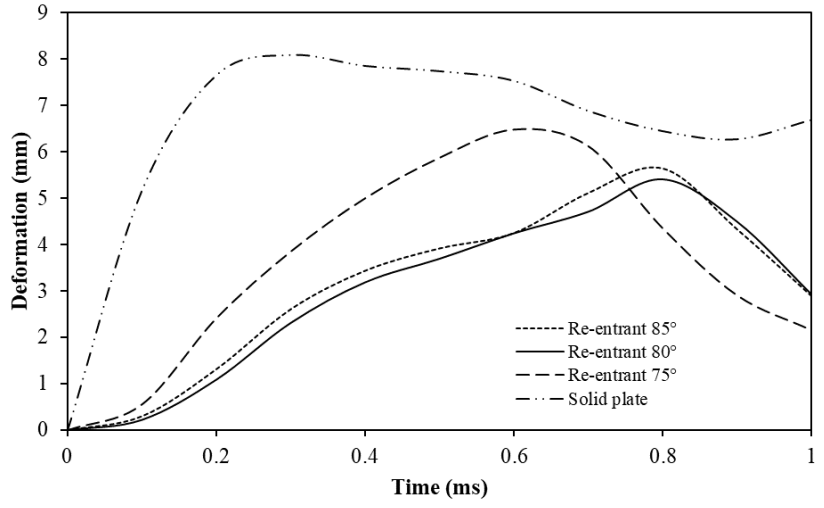


(a)

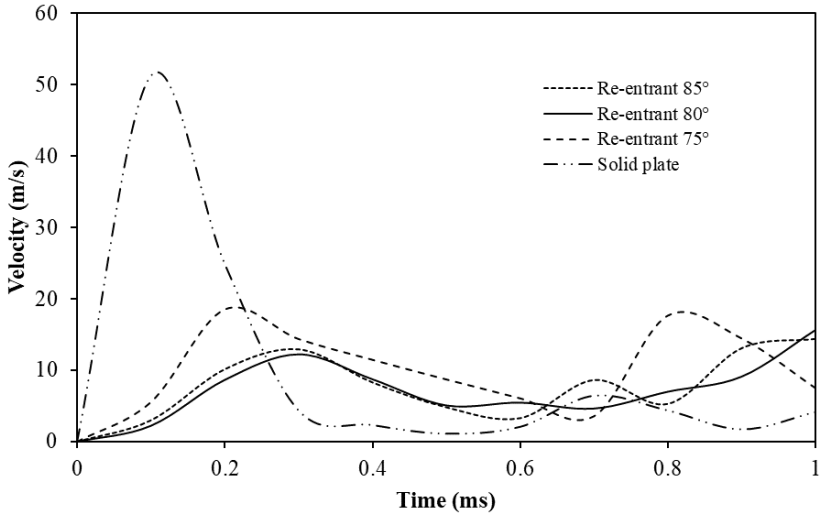


(b)

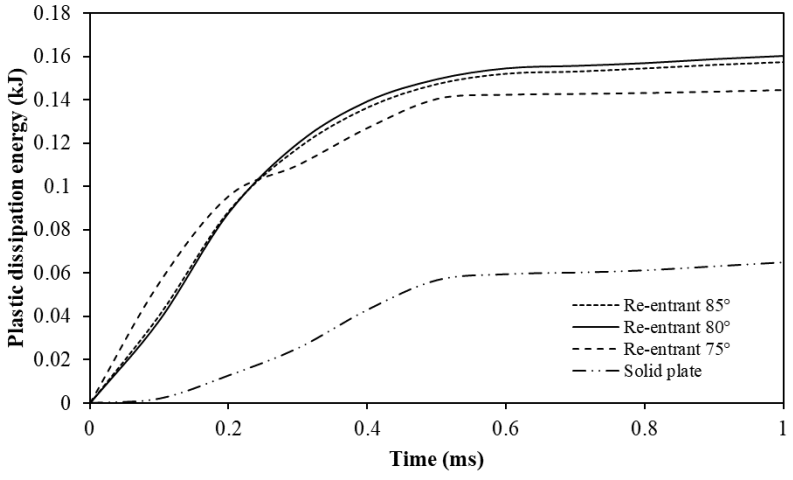


(c)

**Fig 5: Comparison of results among re-entrant structures and solid plate (a) deformations (mm) vs time (ms) profiles, (b) velocities (m/s) vs time (ms) profiles, (c) plastic dissipation energy (kJ) vs time (ms) profiles.**

Among the re-entrant structures, the structure with 80º strut angle plays a significant role in decreasing the deformation of the bottom plate while compared to the solid plate. From these deformation values, the bottom plate velocities are calculated with respect to time for the re-entrant structures and plotted in Fig 5(b). Notably, among the re-entrant structures, 80º strut angle shows better performance in reducing bottom plate velocities while compared with solid plate. Comparing the plastic dissipation energy (Fig 5 (c)), there is no substantial variation with respect to strut angles. While comparing with the solid plate, there is a significant improvement.

*3.1.2. Cumulative Assessment of double re-entrant structures*

In the Figure 6(a), deformations of the bottom plates are depicted for double re-entrant structures with strut angles of 85º, 80º, and 75º as well as for the solid plate.

It is evident from Fig. 6 (a), the 85º strut angle is observed to play a substantial role in the reduction of bottom plate deformations compared to the solid plate. Based on these deformation values, bottom plate velocities are calculated with respect to time for the double re-entrant structures, as illustrated in Fig 6(b). Remarkably, among the double re-entrant structures, 85º strut angle exhibited superior performance in diminishing bottom plate velocities compared to those of the solid plate. While assessing plastic dissipation energy, negligible differences are observed with respect to strut angles among the double re-entrant structures (Fig 6 (c)), but a notable disparity is evident while comparing them with the solid plate.

*3.1.3. Cumulative Assessment of triangular structures*

In the Figure 7(a), the deformations of bottom plates in triangular structures are depicted for different strut angles (85º, 80º, 75º), as well as for the solid plate.

It is clear that within the category of triangular structures, 75º strut angle significantly reduces bottom plate deformations when compared to the solid plate. Fig 7(b) presents the calculated bottom plate velocities against time for these triangular structures. Remarkably, among the triangular structures, 75º strut angle demonstrates superior performance in reducing bottom plate velocities compared to solid plate. While examining plastic dissipation energy, there are minimal differences among all triangular structures (Fig 7 (c)), but a notable contrast emerges when comparing them to the solid plate.

Three distinct auxetic structures, namely re-entrant, double re-entrant, and triangular configurations, are computationally simulated with respective strut angles of 80°, 85°and 75° to evaluate their performance under blast load of 5.57 g of TNT at a standoff distance of 50 mm. Subsequently, these simulations are utilized to generate a graphical representation, depicting the response of these structures across the specified angles. Fig 8 illustrates the optimized results of three distinct auxetic structures for re-entrant 80º, double re-entrant 85º and triangular 75º.

From the obtained data, it is observed that the plastic dissipation energy of triangular 75º structure is greater than the double re-entrant 85º structure. In contrast, the performance of double re-entrant 85º in respect of the deformation of the bottom plate is better compared to triangular structure. Excessive deformation under blast loads may lead to structural failure and results in substantial damage. Therefore, restricting deformation in the structures is pivotal in guaranteeing structural robustness and safety during explosive events. Hence, it is obvious to conclude that the double re-entrant structure with 85º outperforms the other auxetic configurations.

## 4. Parametric exploration of auxetic structures

*4.1. Effect of strut thickness*

In this study, a comprehensive parametric analysis of auxetic structures have been undertaken, encompassing double re-entrant structure with angles of 85°, 80°, and 75°. The primary focus of this investigation is to systematically vary the strut thickness and observe their effects on plastic dissipation energy, deformation and velocity.

Double re-entrant structures, as illustrated in Fig 9, exhibit intriguing behaviour when exposed to blast loads, particularly concerning changes in deformation and plastic dissipation energy, which are influenced by variations in strut thickness. As the thickness of the struts increases, bottom plate deformation also increases and becoming constant after reaching 0.4 mm. On the other hand, the plastic dissipation energy exhibits a decreasing trend. This phenomenon is attributed because of higher structural stiffness, which prevents the structures from experiencing full compression and makes them more rigid in nature.

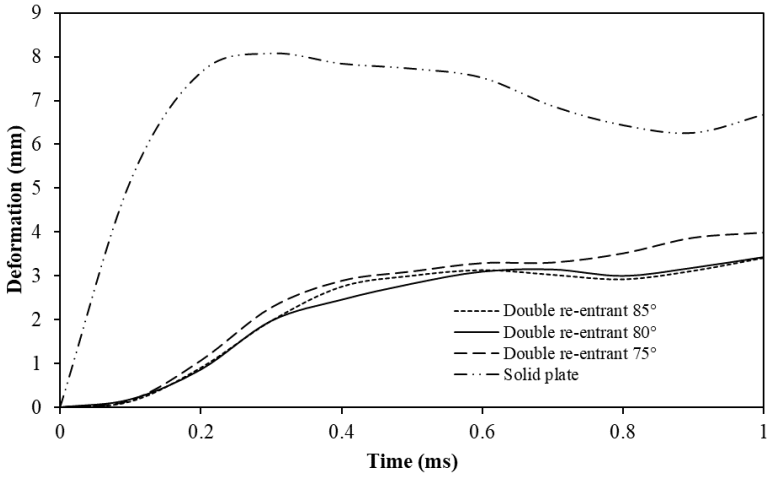


(a)

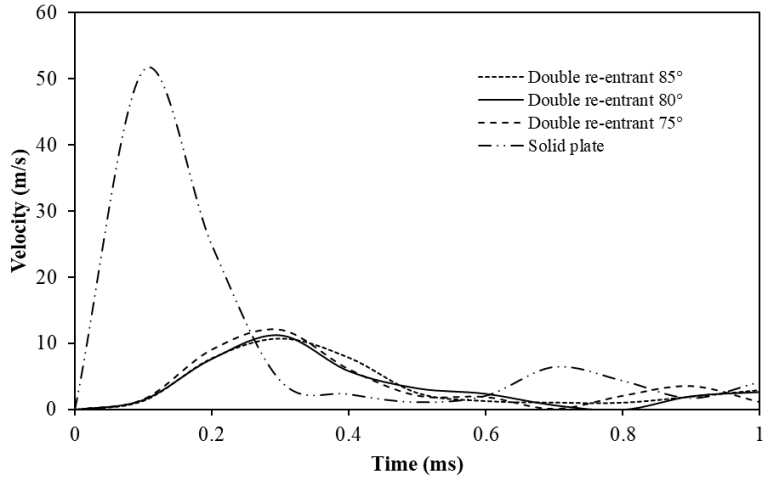


(b)

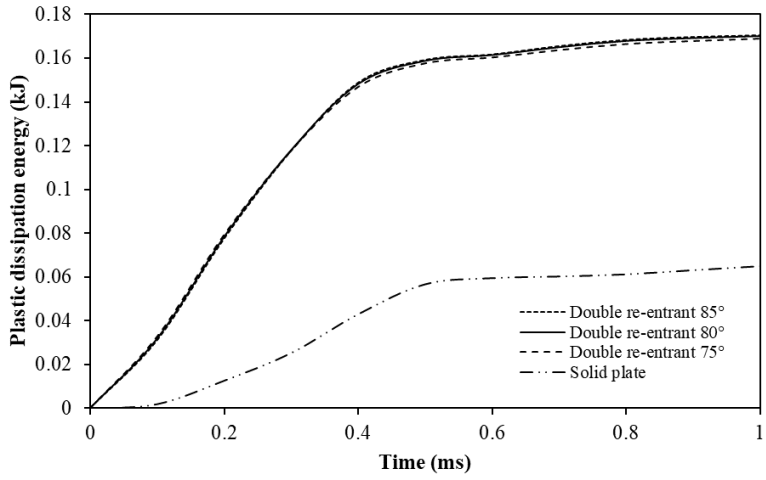


(c)

**Fig 6: Comparison of results among double re-entrant structures and solid plate (a) deformations (mm) vs time (ms) profiles, (b) velocities (m/s) vs time (ms) profiles, (c) plastic dissipation energy (kJ) vs time (ms) profiles.**

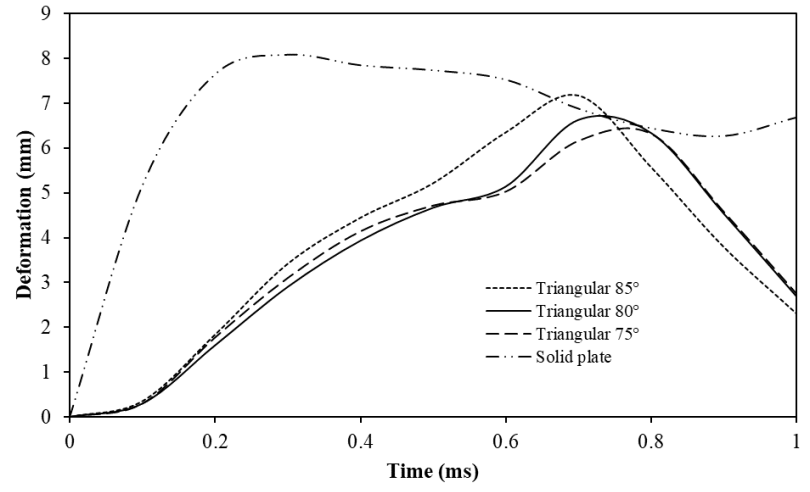


(a)

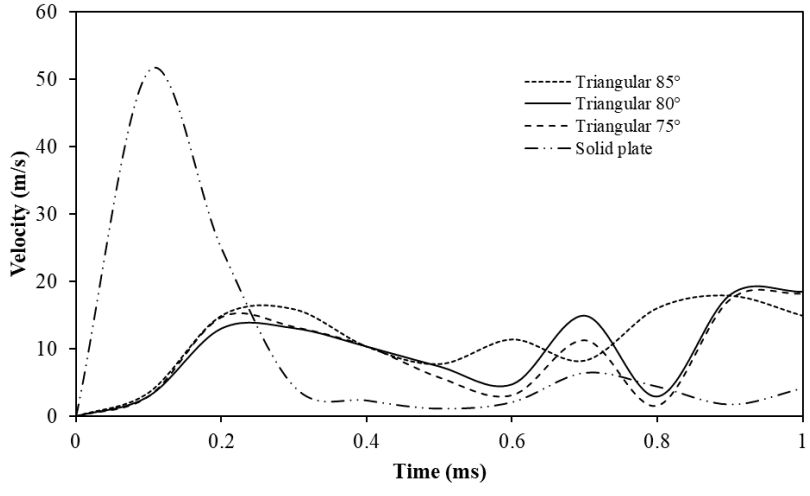


(b)

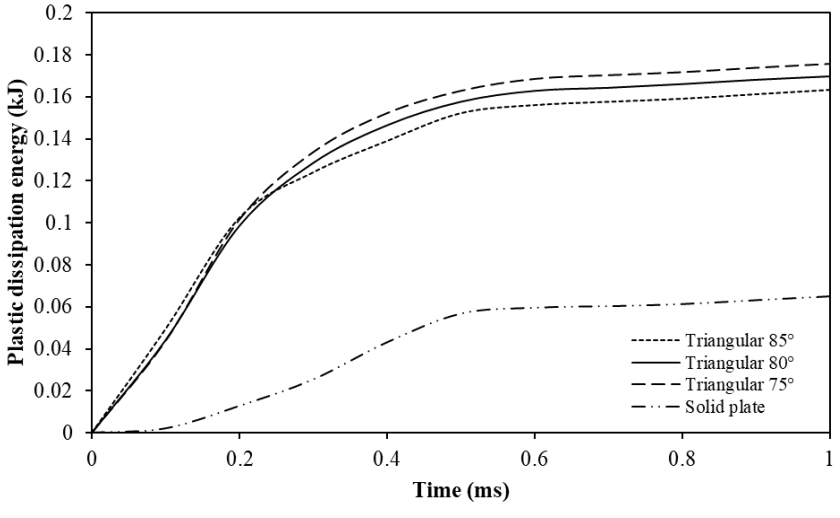


(c)

**Fig 7: Comparison of results among triangular structures and solid plate (a) deformations (mm) vs time (ms) profiles, (b) velocities (m/s) vs time (ms) profiles, (c) plastic dissipation energy (kJ) vs time (ms) profiles.**

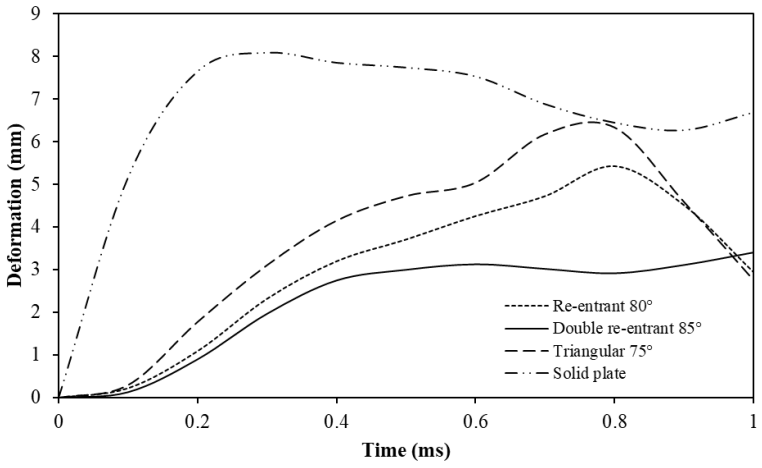


(a)

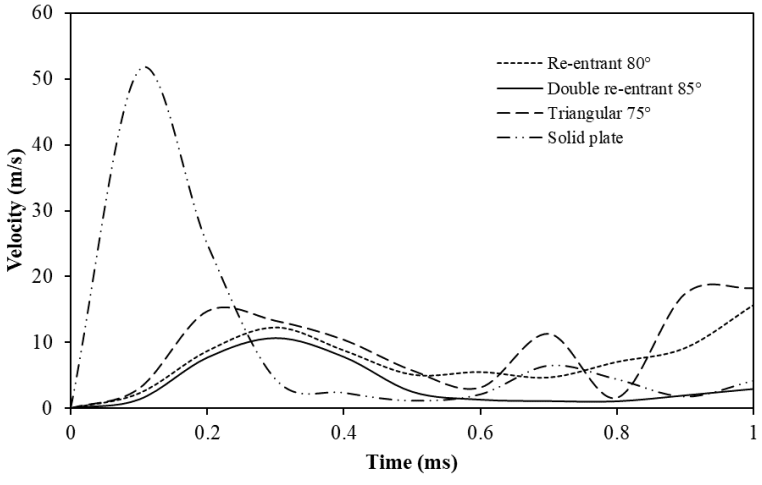


(b)

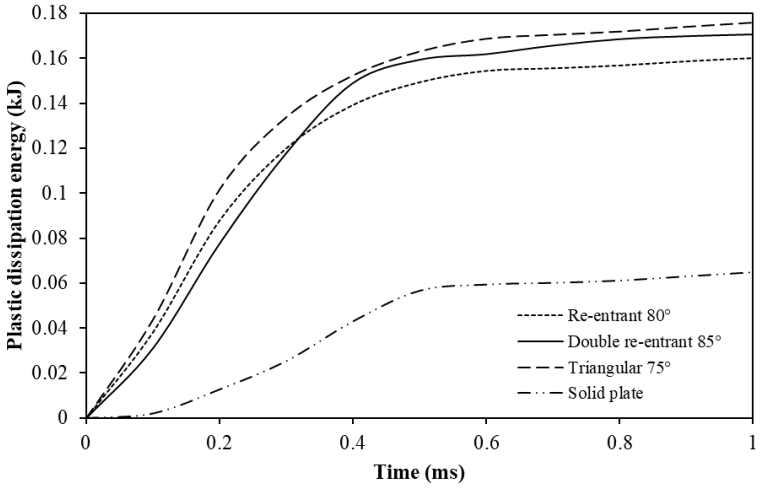


(c)

**Fig 8: Comparison of results among optimized auxetic structures and solid plate (a) deformations (mm) vs time (ms) profiles, (b) velocities (m/s) vs time (ms) profiles, (c) plastic dissipation energy (kJ) vs time (ms) profiles.**

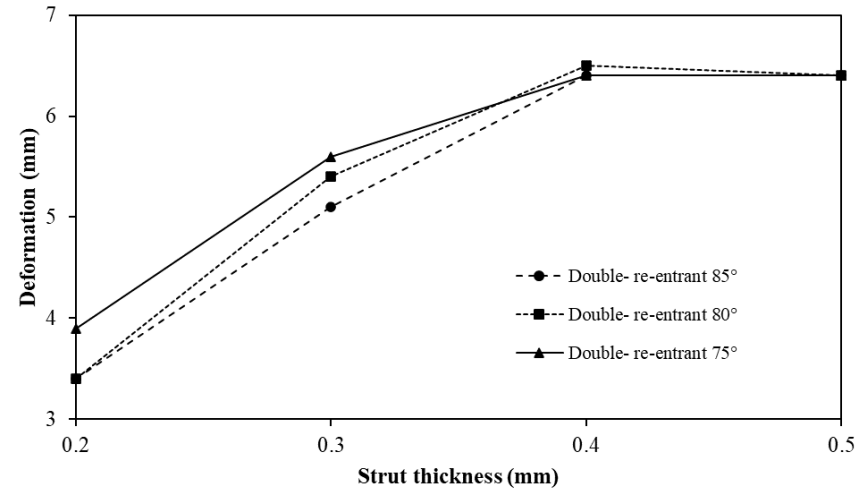


(a)

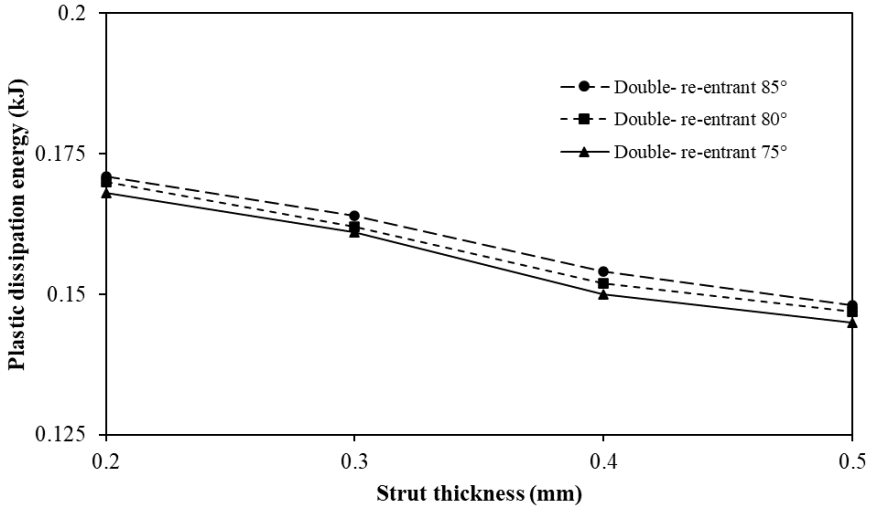


(b)

**Fig 9: Variation of strut thickness for double re-entrant structures, (a) deformation vs strut thickness, (b) plastic dissipation energy vs strut thickness.**

For a comprehensive analysis of three distinct auxetic structures, specifically optimized configurations of re-entrant, double re-entrant, and triangular, computational simulations have been conducted by varying strut thickness. These simulations assessed their response to a blast load equivalent to 5.57 grams of TNT at a 50 mm standoff distance.

In addition, it is evident that increased strut thickness leads to amplified bottom plate deformation, especially in the re-entrant and double re-entrant structures, owing to higher structural stiffness. However, the triangular structures exhibit a reverse trend i.e there is decrement in the deformation and plastic dissipation energy as strut thickness increases. The resulting data is displayed in Fig 10, highlighting optimized outcomes for each structure. Certainly, among the auxetic structures, the double re-entrant structure with 85º strut angle and 0.2 mm strut thickness outperformed than other auxetic structures with a minimal bottom plate displacement of 3.4 mm, and plastic dissipation energy of 0.171 kJ.

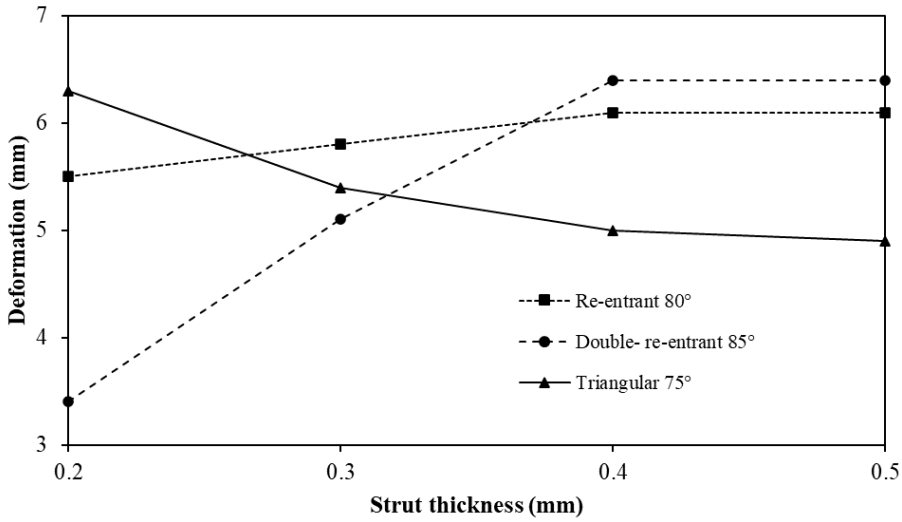


(a)

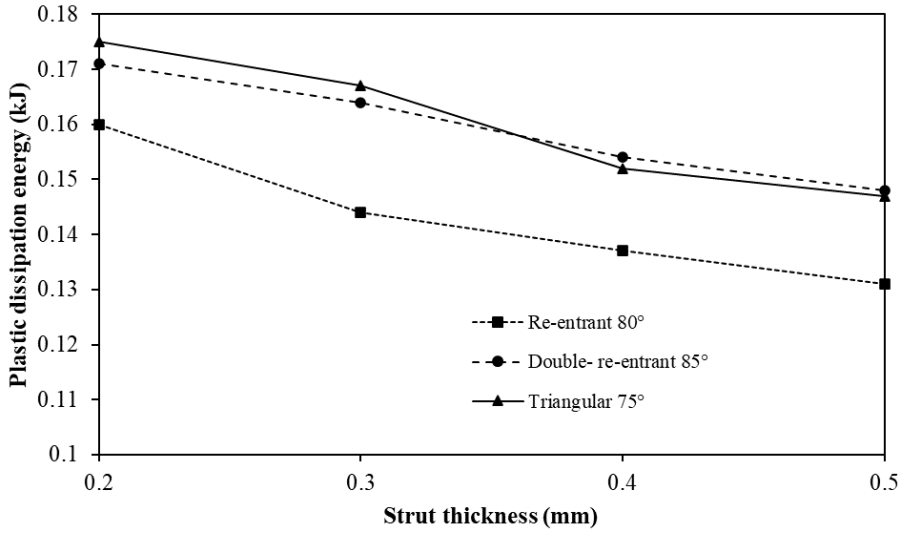


(b)

**Fig 10: Optimized auxetic structures for varied strut thickness, (a) deformation vs strut thickness, (b) plastic dissipation energy vs strut thickness.**

*4.2. Structural consistency with reduced standoff distances*

As the standoff distance decreases, the blast wave reaches the target more rapidly and with greater impulse, potentially leading to heightened damage to the structures. This study aims to examine the influence of varying standoff distances (specifically, reducing it to 30 mm) on the optimized auxetic structures in terms of deformation, velocity, and plastic dissipation energy. The outcomes are plotted and assessed among the structures under the reduced standoff distance 30 mm and compared with 50 mm standoff distance as shown in Fig 11.

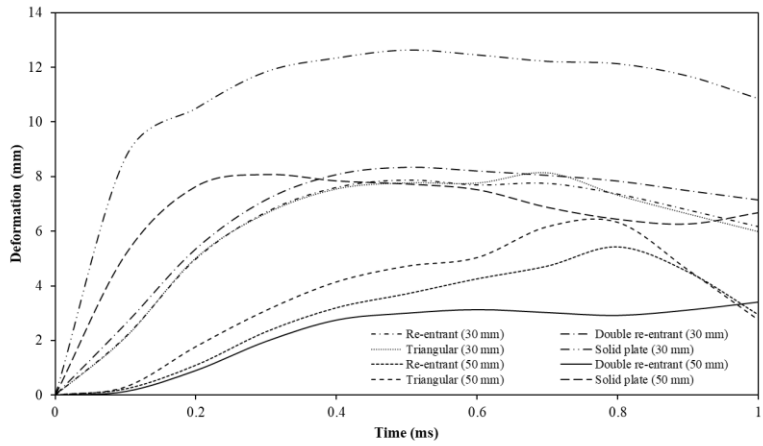


(a)

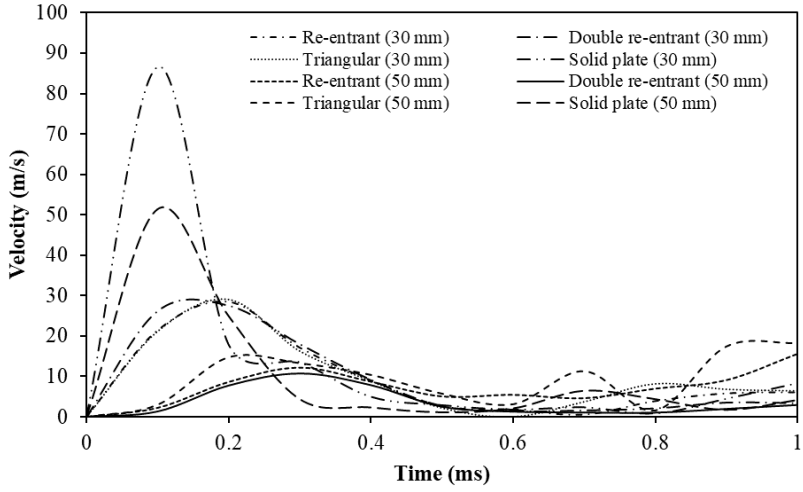


(b)

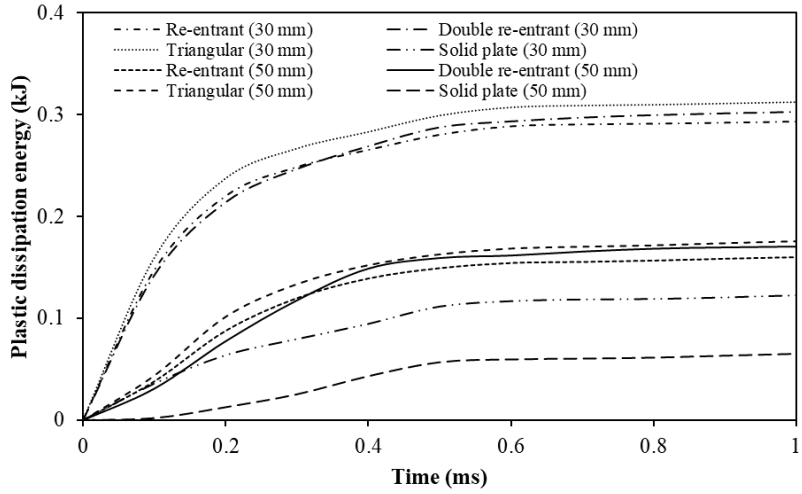


(c)

**Fig 11: Influence of standoff distance among the optimized auxetic structures (a) deformation (mm) vs time (ms) profiles, (b) velocity (m/s) vs time (ms) profiles, (c) plastic dissipation energy (kJ) vs time (ms) profiles at a standoff distance of 30 mm.**

The results indicate increased impulse values appear to quicken the core's compression when standoff distance is 30 mm, resulting in a swift localized densification of the core. However, the deformations, velocities among the

auxetic structures exhibited minimal variation, whereas the solid plate displayed higher deformation. Subsequently, even when the standoff distance is reduced, the auxetic structures especially double re-entrant structure with 85$^o$ strut angle with 0.2 mm strut thickness performed better compared to other auxetic structures and with traditional solid plate. Furthermore, the maximum dissipated energy of auxetic structures consistently performed twice that of a solid plate when subjected to various impulse forces [21].

## 5. Conclusions

This study focused on analyzing the response of auxetic metamaterials with various structural configurations in the context of blast resistance. The study compared the performance of various auxetic structures such as re-entrant, double re-entrant, and triangular with different strut angles (85$^o$, 80$^o$, 75$^o$) and strut thickness against a solid plate. Several key parameters such as bottom plate deformation, velocity, and plastic dissipation energy are examined to assess the effectiveness of these structures in withstanding blast forces.

The initial findings of this investigation revealed that the double re-entrant structure with an 85$^o$ strut angle exhibited the most promising performance among the studied auxetic structures.

To further understand the behavior of these auxetic structures, a parametric study was conducted by varying the strut thickness with a range from 0.2 to 0.5 mm. This investigation revealed that as the strut thickness decreased, the plastic dissipation energy increased. This observation can be attributed to the increased stiffness associated with thicker struts, which in turn led to higher bottom plate deformation. This finding suggests that the design of auxetic structures should carefully balance strut thickness to optimize blast resistance.

Additionally, the standoff distance of the detonation point from the top plate was altered to 30 mm, to understand the consistency of these structures. With a strut thickness of 0.2 mm and varying strut angles (85$^o$, 80$^o$, 75$^o$), the study has been done to find the bottom plate deformation, velocity, and plastic dissipation energy for all optimized auxetic structures and the solid plate. Notably, the auxetic structures demonstrated an approximately threefold increase in energy dissipation compared to the solid plate. This research holds significant implications in the realm of materials engineering, particularly with regard to enhancing safety measures for batteries utilized in Electric Vehicles.

**Conflict of interest:** The authors declare that there is no conflict of interest for this work.

## References

[1] A. A. Zadpoor, Mechanical meta-materials, *Materials Horizons,* Vol. 3, No. 5, pp. 371-381, 2016.

[2] J. O. Cardoso, J. P. Borges, A. Velhinho, Structural metamaterials with negative mechanical/thermomechanical indices: a review, *Progress in Natural Science: Materials International,* Vol. 31, No. 6, pp. 801-808, 2021.

[3] X. Ren, R. Das, P. Tran, T. D. Ngo, Y. M. Xie, Auxetic metamaterials and structures: a review, *Smart materials and structures,* Vol. 27, No. 2, pp. 023001, 2018.

[4] K. K. Saxena, R. Das, E. P. Calius, Three decades of auxetics research− materials with negative Poisson's ratio: a review, *Advanced Engineering Materials,* Vol. 18, No. 11, pp. 1847-1870, 2016.

[5] J. U. Surjadi, L. Gao, H. Du, X. Li, X. Xiong, N. X. Fang, Y. Lu, Mechanical metamaterials and their engineering applications, *Advanced Engineering Materials,* Vol. 21, No. 3, pp. 1800864, 2019.

[6] M. Balan, J. Mertens, M. R. Bahubalendruni, Auxetic mechanical metamaterials and their futuristic developments: A state-of-art review, *Materials Today Communications,* Vol. 34, pp. 105285, 2023.

[7] C. Lu, M. Hsieh, Z. Huang, C. Zhang, Y. Lin, Q. Shen, F. Chen, L. Zhang, Architectural design and additive manufacturing of mechanical metamaterials: a review, *Engineering,* Vol. 17, pp. 44-63, 2022.

[8] X. Yu, J. Zhou, H. Liang, Z. Jiang, L. Wu, Mechanical metamaterials associated with stiffness, rigidity and compressibility: A brief review, *Progress in Materials Science,* Vol. 94, pp. 114-173, 2018.

[9] M. Wan, K. Yu, H. Sun, 4D printed programmable auxetic metamaterials with shape memory effects, *Composite Structures,* Vol. 279, pp. 114791, 2022.

[10] X. Xin, L. Liu, Y. Liu, J. Leng, 4D printing auxetic metamaterials with tunable, programmable, and reconfigurable mechanical properties, *Advanced Functional Materials,* Vol. 30, No. 43, pp. 2004226, 2020.

[11] X. Li, L. Gao, W. Zhou, Y. Wang, Y. Lu, Novel 2D metamaterials with negative Poisson's ratio and negative thermal expansion, *Extreme Mechanics Letters,* Vol. 30, pp. 100498, 2019.

[12] L. Wu, B. Li, J. Zhou, Isotropic negative thermal expansion metamaterials, *ACS applied materials & interfaces,* Vol. 8, No. 27, pp. 17721-17727, 2016.

[13] X. Ren, J. Shen, P. Tran, T. D. Ngo, Y. M. Xie, Design and characterisation of a tuneable 3D buckling-induced auxetic metamaterial, *Materials & Design,* Vol. 139, pp. 336-342, 2018.

[14] L. Ai, X.-L. Gao, Three-dimensional metamaterials with a negative Poisson's ratio and a non-positive coefficient of thermal expansion, *International Journal of Mechanical Sciences*, Vol. 135, pp. 101-113, 2018.

[15] S. Shan, S. H. Kang, Z. Zhao, L. Fang, K. Bertoldi, Design of planar isotropic negative Poisson's ratio structures, *Extreme Mechanics Letters*, Vol. 4, pp. 96-102, 2015.

[16] F. Tarlochan, Sandwich structures for energy absorption applications: A review, *Materials*, Vol. 14, No. 16, pp. 4731, 2021.

[17] Y. Luo, K. Yuan, L. Shen, J. Liu, Sandwich panel with in-plane honeycombs in different Poisson's ratio under low to medium impact loads, *Reviews on Advanced Materials Science*, Vol. 60, No. 1, pp. 145-157, 2021.

[18] G. Imbalzano, P. Tran, T. D. Ngo, P. V. Lee, Three-dimensional modelling of auxetic sandwich panels for localised impact resistance, *Journal of Sandwich Structures & Materials*, Vol. 19, No. 3, pp. 291-316, 2017.

[19] J. Michalski, T. Strek, Response of a sandwich plate with auxetic anti-tetrachiral core to puncture, in *Proceeding of*, Springer, pp. 1-14.

[20] S. Yue, Y. Bai, Z. Du, H. Zou, W. Shi, G. Zheng, Dynamic behavior of kinetic projectile impact on honeycomb sandwich panels and multi-layer plates, *Crystals*, Vol. 12, No. 5, pp. 572, 2022.

[21] G. Imbalzano, P. Tran, T. D. Ngo, P. V. Lee, A numerical study of auxetic composite panels under blast loadings, *Composite Structures*, Vol. 135, pp. 339-352, 2016.

[22] S. M. Soleimani, N. H. Ghareeb, N. H. Shaker, M. B. Siddiqui, Modeling and simulation of honeycomb steel sandwich panels under blast loading, *International Journal of Civil and Environmental Engineering*, Vol. 10, No. 8, pp. 1012-1021, 2016.

[23] K. Zheng, Z. Wang, Numerical investigation on failure behavior of steel plate under explosive loading, *Science China Technological Sciences*, Vol. 64, No. 6, pp. 1311-1324, 2021.

[24] F. Arifurrahman, R. Critchley, I. Horsfall, Experimental and numerical study of auxetic sandwich panels on 160 grams of PE4 blast loading, *Journal of Sandwich Structures & Materials*, Vol. 23, No. 8, pp. 3902-3931, 2021.

[25] H. Lin, C. Han, L. Yang, L. Zhang, H. Luan, P. Han, H. Xu, S. Zhang, Numerical investigation on performance optimization of offshore sandwich blast walls with different honeycomb cores subjected to blast loading, *Journal of Marine Science and Engineering*, Vol. 10, No. 11, pp. 1743, 2022.

[26] S. Yao, Z. Wang, D. Zhang, F. Lu, N. Zhao, Y. Wang, Damage evaluation and prediction of steel box structures under internal blast, *Journal of Mechanical Science and Technology*, Vol. 36, No. 10, pp. 5125-5133, 2022.

[27] N. Novak, L. Starčevič, M. Vesenjak, Z. Ren, Blast response study of the sandwich composite panels with 3D chiral auxetic core, *Composite Structures*, Vol. 210, pp. 167-178, 2019.

[28] H. N. Wadley, K. P. Dharmasena, M. He, R. M. McMeeking, A. G. Evans, T. Bui-Thanh, R. Radovitzky, An active concept for limiting injuries caused by air blasts, *International Journal of Impact Engineering*, Vol. 37, No. 3, pp. 317-323, 2010.

[29] A. Montazeri, A. Saeedi, E. Bahmanpour, M. Safarabadi, Enhancing the compressive properties of re-entrant honeycombs by line defects with insight from nature, *Materials Today Communications*, Vol. 38, pp. 107700, 2024.

[30] M. R. Hajighasemi, M. Safarabadi, A. Sheidaei, M. Baghani, M. Baniassadi, Design and manufacture of a smart macro-structure with changeable effective stiffness, *International Journal of Applied Mechanics*, Vol. 12, No. 01, pp. 2050001, 2020.

[31] A. Montazeri, A. Hasani, M. Safarabadi, Bending performance and failure mechanism of 3D-printed hybrid geometry honeycombs with various poisson's ratios, *Journal of Sandwich Structures & Materials*, Vol. 25, No. 7, pp. 709-729, 2023.

[32] M. H. Fatahi, M. Hamedi, M. Safarabadi, Experimental and numerical implementation of auxetic substrate for enhancing voltage of piezoelectric sandwich beam harvester, *Mechanics of Advanced Materials and Structures*, Vol. 29, No. 27, pp. 6107-6117, 2022.

[33] D. Prakash, G. Jeyakumar, A Review of Problem Variants and Approaches for Electric Vehicle Charging and Location Identification, *Research Reports on Computer Science*, pp. 65-76, 2023.

[34] O. f. B. D. M. A. C. S. o. T.-w. C. i. C. City, V. Athira, Kichu Mariam John and L. Nitha, *International Journal of Pure and Applied Mathematics*, Vol. 119, No. 10, pp. 759-774, 2018.

[35] B. Rohini, D. M. Pavuluri, N. K. LS, V. Soorya, N. Mohankumar, Technology Manoevering in Smart Vehicles for Safe Commute, in *Proceeding of*, IEEE, pp. 617-622.

[36] A. J. Damahe, C. Sumesh, A. Ramesh, Empirical relationship for fracture energy in machining processes: a FEM-based investigation with AISI 1045 steel, *International Journal on Interactive Design and Manufacturing (IJIDeM)*, pp. 1-9, 2023.

[37] A. Ramesh, C. Sumesh, P. Abhilash, S. Rakesh, Finite element modelling of orthogonal machining of hard to machine materials, *International Journal of Machining and Machinability of Materials*, Vol. 17, No. 6, pp. 543-568, 2015.

[38] V. Karlos, G. Solomos, Calculation of blast loads for application to structural components, *Luxembourg: Publications Office of the European Union*, Vol. 5, 2013.

[39] C. Zhao, J. Sun, Q. Wang, Thermal runaway hazards investigation on 18650 lithium-ion battery using extended volume accelerating rate calorimeter, *Journal of Energy Storage*, Vol. 28, pp. 101232, 2020.